

Article

High Temperature Low Friction Behavior of h-BN Coatings against ZrO₂

Qunfeng Zeng 

Key Laboratory of Education Ministry for Modern Design and Rotor-Bearing System, Xi'an Jiaotong University, Xi'an 710049, China; zengqf1949@gmail.com

Abstract: This paper presents high temperature low friction behaviors of the h-BN coatings, which were deposited on high-speed tool steel by radio frequency magnetron sputtering. A tribometer was used to investigate high temperature tribological properties of h-BN coatings against ZrO₂ from 500 °C to 800 °C. The surface morphology, mechanical properties and chemical states of the worn surface of the friction pair were characterized and investigated systemically. The experimental results show that h-BN coatings are of significant importance to improve high temperature tribological properties of steel. Moreover, it is found that high temperature super low friction of the friction pairs is successfully achieved due to tribochemistry, which plays a key role in forming the in-situ generated Fe₂O₃/h-BN composites on the worn surface of h-BN coatings. CoFs of the friction pair are as super low as about 0.02 at 800 °C and around 0.03 at 600 °C at the stable stage. The high temperature super low friction mechanism of the friction pair is discussed in detail. The present study opens a new strategy to achieve high temperature super low friction of the friction system during sliding.

Keywords: hexagonal boron nitride coatings; in-situ generated composite; tribochemistry; high temperature low friction



Citation: Zeng, Q. High Temperature Low Friction Behavior of h-BN Coatings against ZrO₂. *Coatings* **2022**, *12*, 1772. <https://doi.org/10.3390/coatings12111772>

Academic Editor: Sergey N. Grigoriev

Received: 17 October 2022

Accepted: 16 November 2022

Published: 19 November 2022

Publisher's Note: MDPI stays neutral with regard to jurisdictional claims in published maps and institutional affiliations.



Copyright: © 2022 by the author. Licensee MDPI, Basel, Switzerland. This article is an open access article distributed under the terms and conditions of the Creative Commons Attribution (CC BY) license (<https://creativecommons.org/licenses/by/4.0/>).

1. Introduction

In recent years, many high-end pieces of equipment have been working under high operating temperature in industrial applications such as hot metal forming and aerospace [1,2]. The beneficial lubrication of self-lubricating materials may be lost due to high temperature friction heating during sliding contact in addition to high environmental temperature. How to achieve good lubrication performances of the friction system at high temperature has become a very urgent tribological problem [3–5]. The lubricating oils and greases have good lubricating performances at ambient temperature, but the lubrication performance is reduced or even completely fails due to the decomposition or deterioration of the lubricating oils and greases at high temperature especially in extremely harsh environments [6,7]. The operating temperature of the machine parts in the field of hot metal forming and aerospace is higher than 300 °C. There is observable oxidation, even failure, of high performance solid lubricants, such as DLC films, around 300 °C [8–10]. Therefore, other solid lubricants, such as 2D materials, are proposed to improve the lubrication performances of the machine parts above 300 °C [11,12]. The friction heating of the friction pair is frequently generated during sliding and a tribochemical reaction at the interface of the friction pair is found at the worn surface and a tribofilm may be formed, improving the tribological properties of the friction pair. This layer of tribofilm as a protective film separates the two rubbing surfaces from direct contact reducing friction and wear. However, many solid lubricants (e.g., graphite, MoS₂ and WS₂) can be degraded or oxidized in ambient air at high temperature [13–15].

Hexagonal boron nitride (h-BN) exhibits a good combination of the properties of high chemical stability, high mechanical strength, high thermal conductivity and low density of surface dangling bonds. The h-BN has a lamellar crystal structure and is served as solid lubricant with low coefficient of friction (CoF), even superlubricity [16–21]. The h-BN as

solid lubricant is used in two ways. One is that h-BN powders are used as solid lubricants in the metal or ceramic matrix materials. Chen et al. studied the friction behaviors of the SiC/h-BN composites with different volume fractions of h-BN from room temperature to 900 °C [22]. The ZrO₂/h-BN/SiC composite exhibits good lubricating behaviors, as low as below 0.3 of CoF above 800 °C [23]. CoF and wear rate of Ag/h-BN-containing Ni-based composites were found to decrease with the increasing temperature from room temperature to 600 °C [24]. TiB₂ and TiN playing a role in the wear-resistance were synthesized in situ in the Ni60/h-BN coatings on Ti-6Al-4V alloys during high power laser irradiation, and the metal oxides (TiO₂, Al₂O₃, NiO and Fe₂O₃) were synthesized in situ during high temperature sliding, exhibiting good anti-friction behavior at 600 °C [25]. The h-BN powders were used to the sliding interface of Si₃N₄ against die steel H13 at 800 °C. The anti-wear behaviors of h-BN lubricating film are featured to the gradual undermining and complete damage [26]. Moreover, h-BN has been found to perform worse than graphite in terms of friction and material transfer in high temperature aluminum forming [27]. The other way is that h-BN is used as solid lubricant coating with good tribological properties for the sliding components made of the substrate steels at high temperature [28,29]. The h-BN coating prepared from a polyborazylene (PBN) polymeric precursor was deposited on titanium-based substrates and annealed via infra-red irradiation in a rapid thermal annealing (RTA) furnace. CoF was reduced from 0.72 for the Ti/stainless tribosystem to 0.35 for the Ti/h-BN/stainless tribosystem at 360 °C [19]. The tribological characteristics of single-layer h-BN were investigated to elucidate the feasibility as a protective coating layer and solid lubricant for micro- and nano-devices. The results indicate that the friction of h-BN before failure was orders of magnitude smaller than that of a SiO₂/Si substrate and the feasibility of atomically thin h-BN as a protective coating layer and solid lubricant [30]. It is well known that the tribological properties are strongly dependent on the operating parameters including temperature and counterpart materials [31–33]. However, the limited papers discussed the anti-friction mechanism of h-BN coatings at high temperature.

In the present paper, the h-BN coatings were deposited on the high-speed tool steel by radio frequency magnetron sputtering method, and the tribological properties of the friction pair of h-BN coatings on the disc against ZrO₂ ball in the range of temperatures from 500 °C to 800 °C was systemically studied. The anti-friction behaviors and mechanisms of the friction pair at high temperature are systemically discussed.

2. Experimental Details

The h-BN coatings were deposited on the high-speed tool steel discs by radio frequency magnetron sputtering system in an Ar atmosphere with an h-BN target ($\Phi 76.2 \times 3$ mm with the purity of 99.9% and the back target of the copper with the thickness of 2 mm, Quanzhou Qijin New Material Technology Co. Ltd., Quanzhou, China). The chamber was pumped to 2×10^{-5} Pa prior to deposition. The heat treatment of the steel is the heating quenching and tempering. The steel discs, which is steel with high hardness, high wear resistance and high heat resistance, were polished by SiC paper with 400#, 600#, 800#, 1200#, 1500# and 2400# and chenille sandpaper to surface roughness around 0.02 μm . The discs with a radius of 30 mm and a height of 5 mm were ultrasonically cleaned around 10 min with absolute ethanol before sputtering. The substrates were mounted on the rotating sample holder. The sample holder was mounted motionless during the deposition. The distance between the target and the target was around 20 mm. The steel discs were firstly etched for 10 min by Ar ions to remove the contamination on surface. Then, Ti intermediate layer of 100 nm in thickness was prepared to enhance the bonding strength between the coatings and steel substrate by Ti target ($\Phi 76.2 \times 3$ mm, purity of 99.995%, Zhongnuo Advanced Material Co. Ltd., Beijing, China). Ti intermediate layer buffers the lattice matching and stress between the BN layer and steel surface, and the intermediate layer can improve the service life of the h-BN coatings. Finally, h-BN coatings were deposited for 180 min at 300 °C and the flow rate was about 15 sccm. The power was 300 W. The thickness of h-BN coatings was about 600 nm. A ZrO₂ ball of 9.5 mm diameter was used as a rubbing pair.

The tribotests were performed by the tribometer at different temperatures. The samples were ultrasonically cleaned with absolute ethanol for 10 min and dried with dry air before tribotests. The load is 2 N and the sliding speed was 0.1 m/s for all tribotests in order to ensure the same friction environmental conditions. The Poisson's ratio and elastic modulus of ZrO₂ ball were 0.3 and 220 GPa and the Poisson's ratio and elastic modulus of the steel were 0.3 and 206 GPa, the maximum contact pressure was about 0.95 GPa according to the Hertz contact theory. All friction tests were repeated three times to obtain a high level of reproducibility of results. The testing temperatures were 500 °C, 600 °C, 700 °C and 800 °C. The samples were heated to the preset temperature and maintained at this temperature for 15 min to make sure the heating balance and eliminate the effect of the thermal deformation of the substrate and coatings. Then, load was applied to the samples, the tribotest was conducted and data was recorded. A new sample was cleaned and used for each tribotest condition to compare the experimental results.

The microstructure of h-BN coatings was studied by X-ray diffraction (XRD, D8-Advance, Bruker, Saarbrücken, Germany) with a scan rate of 0.5° per second in the range of 2 θ from 20–90°. Scanning electron microscope (SEM, MALA3 LMH, TESCAN, Brno, Czech) and Laser scanning confocal microscopy (LSCM, OLS4000, Olympus, Tokyo, Japan) were used to observe the morphologies of the worn surface and the depth of the wear scar, and the wear rate of the coatings was calculated after tribotests. After the tribotesting, SEM was immediately used to observe the morphologies of the worn surface.

The mechanical properties of h-BN coatings were studied using the nanoindentation test method to measure elastic modulus and hardness by a nanoindentation tester (Ti950, Hysitron, Eden Prairie, Hennepin, MN, USA) with a Berkovich diamond indenter. The effective tip radius was 50 nm and the indenter depth was 55 nm. The loading and unloading were both carried out at a constant indentation speed of 5 nm/s, and the loading time and the unloading time were both 11 s. In order to eliminate the influence of the substrate on the hardness and elastic modulus of h-BN coating, the indentation depth was larger than 10% of the actual thickness of h-BN coating. Scratch testing was carried out on the sample using the micro scratch tester. The tester was used as a progressive loading device. The initial load was 0, the final load was 5 N and a loading rate of 50 N/mm was used for the scratch tests. The friction force was measured and an accelerometer detected the acoustic emission produced as the coating is damaged. The value of the critical load was then determined using these traces in conjunction with an optical microscope. Surface roughness is most important in influencing friction. The surface morphology and roughness of h-BN coating was observed and characterized by atomic force microscope (AFM, Innova, Bruker, Saarbrücken, Germany). Raman spectroscopy with 633 nm He-Ne laser excitation source and 1 cm⁻¹ resolution (HR800, Horiba Jobin Yvon, Paris, France) was used to analyze the microstructure and surface morphology of the friction pair.

3. Results and Discussion

Figure 1 shows the XRD pattern of h-BN coatings. The characterization diffraction peaks at 28°, 41° and 43° were detected, and assigned to (002), (100) and (101) crystallographic planes of h-BN, respectively. These particles are crystalline in coatings with sizes in the range of 80–120 nm calculated by the Debye-Scherrer equation [34]. The peaks at 45°, 65° and 82° are the characteristic peaks of Fe from the steel substrate. The three peaks at 37°, 44° and 73° maybe the characteristic peaks of Fe₃O₄. Moreover, the weak peak at 46° about TiO₂ phase is also observed in the XRD pattern corresponding to TiO₂ (004) phase from Ti intermediate layer. The weak peak at 35° is due to the presence of γ -Fe₂O₃ phase matched with the standard [35]. It is clearly concluded from the measurement of XRD that h-BN coatings are prepared on the steel substrate and there is also γ -Fe₂O₃, Fe₃O₄ and TiO₂ on the steel surface. The magnetron sputtering is a clean process. However, the sputtering temperature is around 300 °C, the steel substrate maybe oxidized to Fe₂O₃, Fe₃O₄ and Ti to Ti-O in the coating. These peaks of Fe₂O₃, Fe₃O₄ and Ti-O in XRD are relatively weak, which means there are only a few in the coating. Figure 2 shows the surface

topography of h-BN coatings scanned on the area of $10\ \mu\text{m} \times 10\ \mu\text{m}$ sizes, which gives an indication of the height and depth dimensions of h-BN coatings in AFM images. The peak-to-valley roughness was found in the range of 5–15 nm. The surfaces of h-BN coatings were slightly smooth.

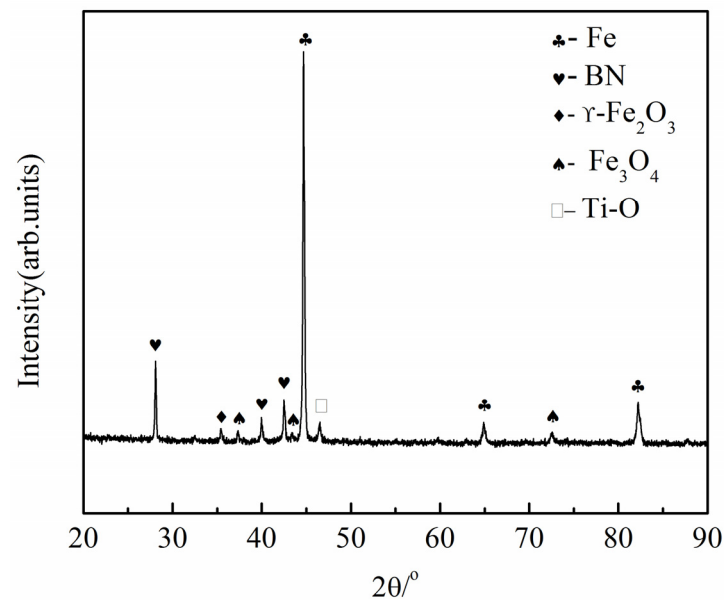


Figure 1. XRD of h-BN coatings.

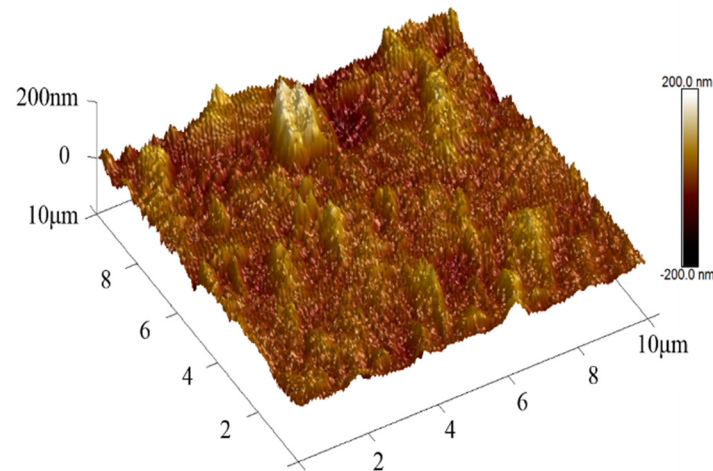


Figure 2. AFM image of h-BN coatings.

Figure 3 shows the loading-unloading curve of h-BN coatings. The h_f and h_{max} are the residual indentation depth and the maximum indentation depth, respectively. The P_{max} is the peak load at h_{max} . The results show that the hardness of the coatings is 3.42 GPa, the elastic modulus is 46.29 GPa, and the H/E value of the coating is 0.074. It is found that the maximum displacement of h-BN coatings is 55.5 nm and h_f is 8 nm, and the elastic recovery rate is 85.6%. It is well known that the large recoverable strain is important for improving the tribological properties of the friction system apart from high H/E value because large recoverable strain is restored at initial state.

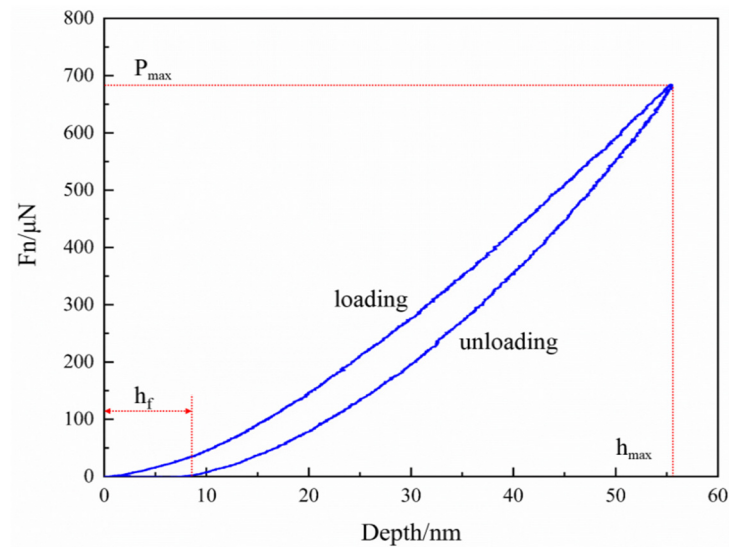


Figure 3. The representative load-depth curves of h-BN coatings.

Figure 4 shows the surface topography and the acoustic emission signal of scratches of h-BN coatings. The initial load is 0, the final load is 5 N and the loading rate is 50 mN/s. The total length of the scratch is set to 2 mm. The force L_{c1} of BN coatings was measured. It is found from the curve that the acoustic emission signals begin to fluctuate when the load is 2.3 N, meaning that this load reaches the critical load of h-BN coatings. The acoustic emission signal of the indenter prior to the critical load is very weak and h-BN coatings are peeled off slightly from the scratch morphology. The indenter was penetrated to h-BN coatings and even contacted the transition layer or the substrate with the increase in load.

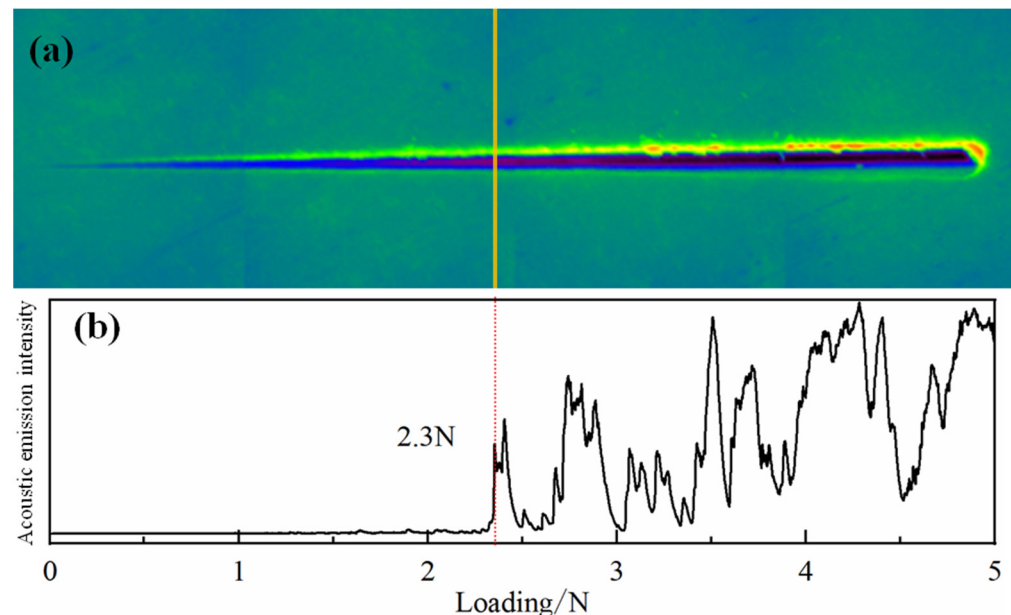


Figure 4. Detailed analysis of h-BN coatings. (a) microscopic record, (b) the acoustic emission record showing the critical load of the coatings first penetration.

Figure 5 shows the CoF curves of h-BN coatings in the atmospheric environment from 500 to 800 °C. The tendency of the CoF curve is different in each CoF curve among all the temperatures according to Figure 5. Figure 6 shows the details of the CoF curves of h-BN coatings in the atmospheric environment from 500 to 800 °C. It shows that h-BN coatings are beneficial to improve high temperature antifriction behaviors of steel. The

tendency of the CoF curve is slightly different although all initial CoFs are the maximum value in each CoF curve among all the temperatures. At 500 °C, CoF decreased first and then increased slightly with the increase in sliding time. The initial CoF was 0.39 at 500 °C, and then decreased gradually, and the average CoF was around 0.13 at the steady stage. At 600 °C, the initial CoF was around 0.48, and then decreased to a low value; however, this CoF value at the same time was little higher than that at 500 °C. At about 150 s, CoF reached around 0.45 at 610 s, and finally decreased around 0.05, as shown in Figure 6b. At 700 °C, CoF decreased from 0.3 to 0.05 for the period of 140 s, and then fluctuated with the sliding time, average CoF was about 0.07. At 800 °C, CoF was as high as 0.72 in the initial stage, and then decreased and increased alternately fluctuations, and CoF reached to the minim value of 0.017 around 1800 s, and then CoF increased again with the increase in the remaining sliding time.

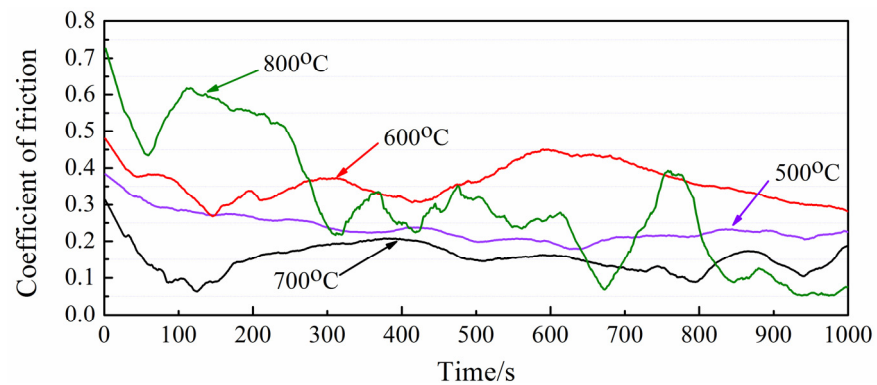


Figure 5. CoF of h-BN coatings under different temperatures.

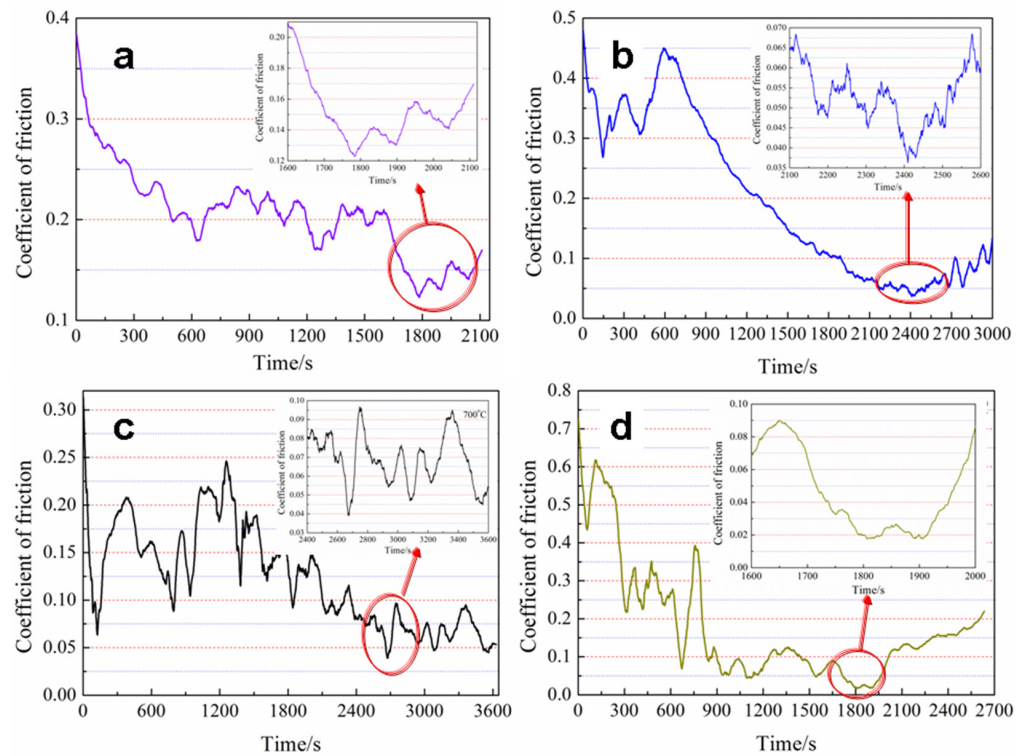


Figure 6. CoF of BN coatings under different temperatures in details: (a) 500 °C, (b) 600 °C, (c) 700 °C and (d) 800 °C.

Figure 7 shows the average CoF of the uncoated steel and h-BN coatings on the steel under different temperatures. CoFs of the uncoated steel are also listed in the reference [3].

It is found that CoFs of the steel decrease and CoFs of h-BN coatings decrease first and then fluctuate from 500 °C to 800 °C. Moreover, CoFs of h-BN coatings are much lower than those of the uncoated steel at the same temperature. It is of interest that h-BN coatings exhibit high temperature superlubricity at 800 °C.

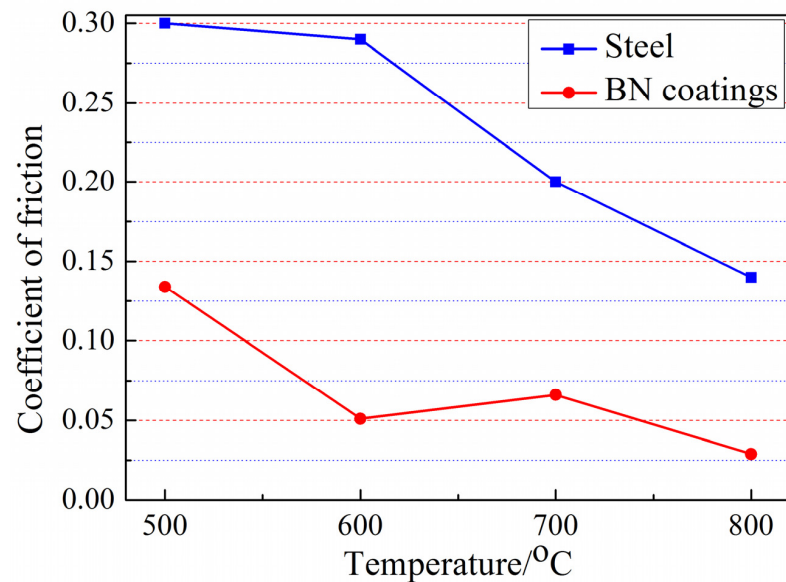


Figure 7. CoF of the uncoated steel and h-BN coatings under different temperatures.

Figures 8 and 9 show the surface topography of the worn surface of the friction pair, respectively. There was an obvious circle wear scar and wear debris on the ball surface. The wear debris were not only adhered to the worn surface and but also pushed on the edge of the worn surface along the sliding direction. The widths of disc are 818 μm , 1163 μm , 909 μm and 788 μm and the widths of ZrO₂ ball are 831 μm , 1273 μm , 918 μm , and 1202 μm from 500 °C to 800 °C, respectively.

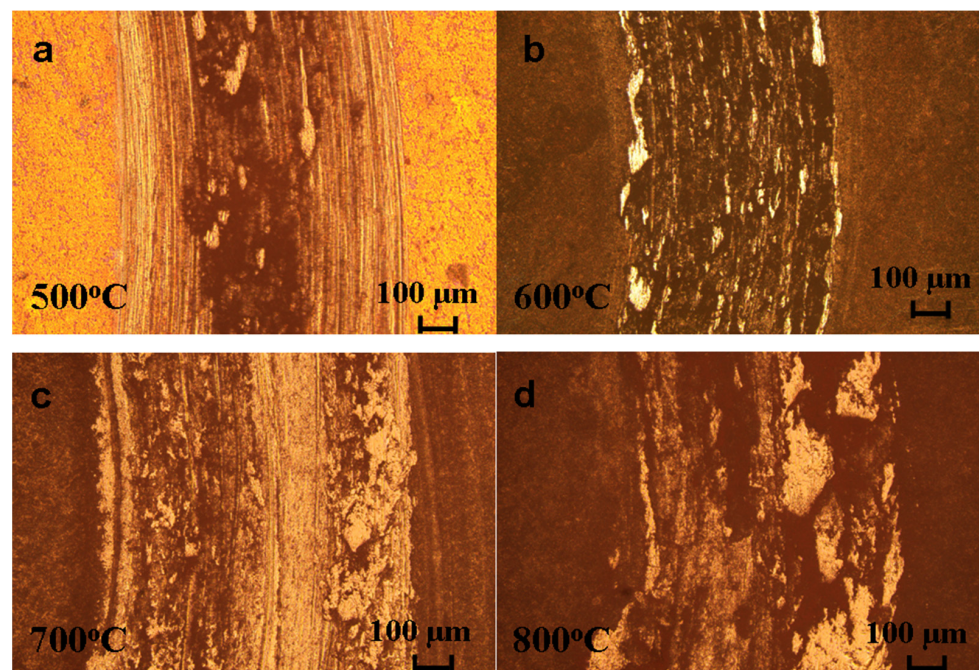


Figure 8. Optical images of flat worn surface under different temperatures: (a) 500 °C, (b) 600 °C, (c) 700 °C and (d) 800 °C.

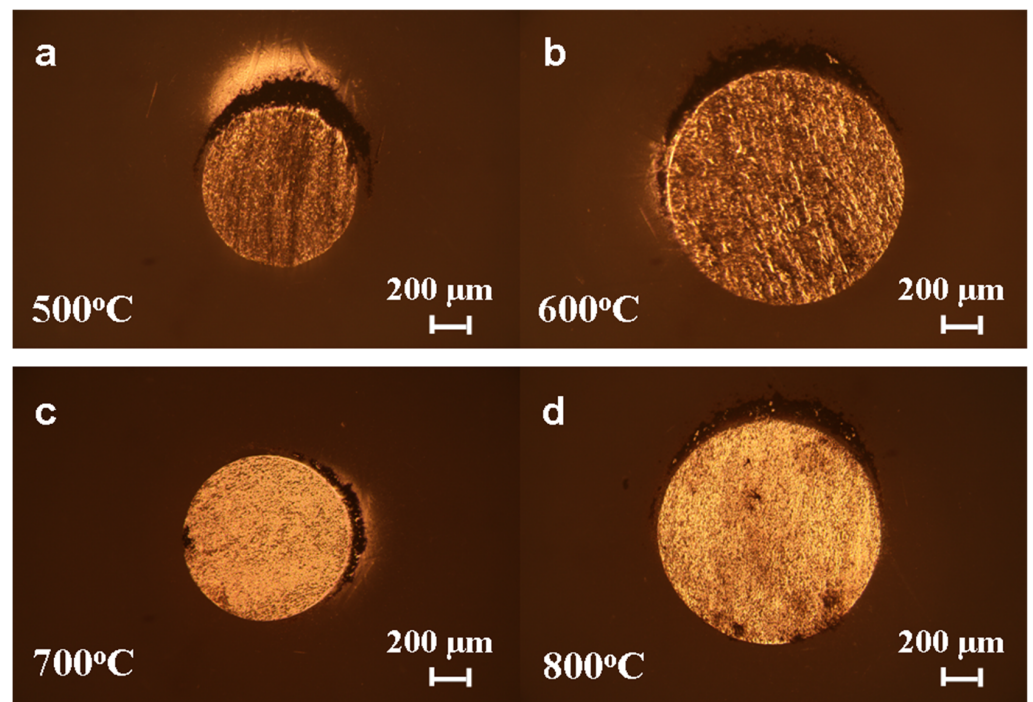


Figure 9. Optical images of ZrO_2 ball worn surface under different temperatures: (a) 500 °C, (b) 600 °C, (c) 700 °C and (d) 800 °C.

On the worn surface topography of disc, there was obvious adhesion wear on the wear scars from 500 to 800 °C, as well as abrasive wear at the temperatures of 600–800 °C. There was a wear scratch on the worn surface of disc along the sliding direction and the corresponding scratch on ball at 600 °C.

The three-dimensional morphology of the worn surface on the steel disc was observed with a laser confocal microscope, as shown in Figure 10. The wear rate of h-BN coatings was calculated according to the cross-sectional area of the worn surface at each temperature. The wear rates are $2.89 \times 10^{-4} \text{ mm}^3 (\text{Nm})^{-1}$, $1.5 \times 10^{-4} \text{ mm}^3 (\text{Nm})^{-1}$, $4.01 \times 10^{-5} \text{ mm}^3 (\text{Nm})^{-1}$ and $7.25 \times 10^{-5} \text{ mm}^3 (\text{Nm})^{-1}$ from 500 to 800 °C. It is found that the depth is large, although the width of the wear scar of ball and disc is narrower at 500 °C, and the wear rate is high.

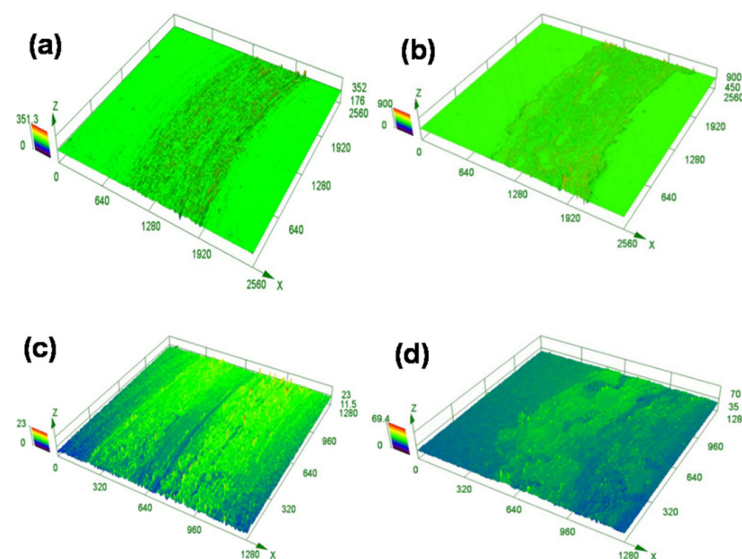


Figure 10. Three-dimensional images of the worn surface of BN coatings under different temperatures: (a) 500 °C, (b) 600 °C, (c) 700 °C and (d) 800 °C.

The wear scar of h-BN coatings was measured by XRD to discuss the friction mechanism of the friction pair at high temperature. Figure 11 shows the XRD pattern of the wear scar of h-BN coatings under different temperatures. It was found that there was h-BN and α -Fe₂O₃ in the worn surface of disc under different temperatures. The steel substrates were easily oxidized in ambient environment once h-BN coatings were worn out or destroyed during sliding. There was a small amount of boron oxide in the wear scar, which is helpful to reduce friction at the temperatures of 500 °C, 700 °C and 800 °C. However, there was no boron oxide measured in the worn surface of disc at 600 °C, although CoF is low at the steady stage. Moreover, it was found that there was γ -Fe₂O₃ in the worn surface at 800 °C.

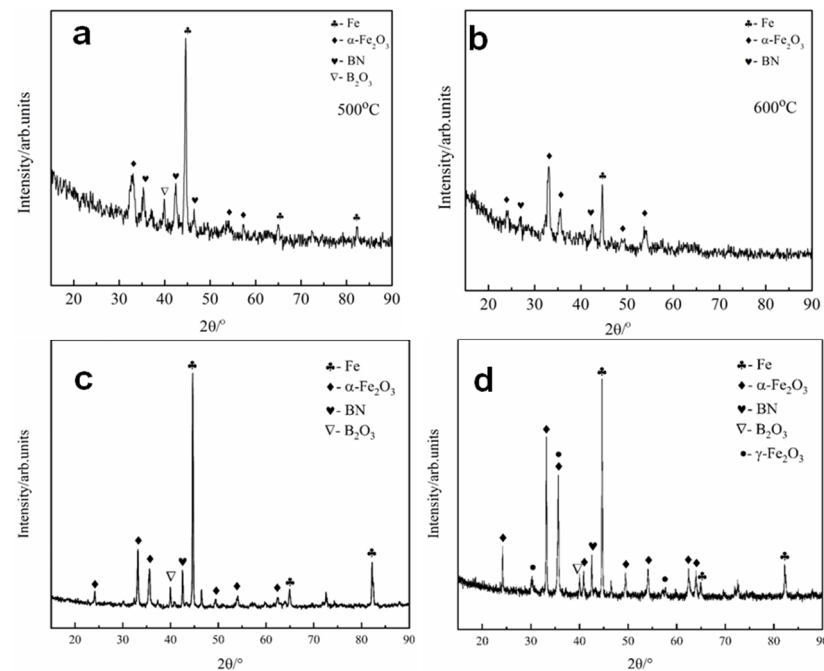


Figure 11. XRD of the worn surface of h-BN coatings under different temperatures: (a) 500 °C, (b) 600 °C, (c) 700 °C and (d) 800 °C.

The wear scar of h-BN coatings was observed by SEM, as shown in Figure 12. At 500 °C, there was a compacted layered material around the center of the wear scar, and there were also block products. At 600 °C, there was a lot of granular debris at the wear scar, while needle-like wear debris appeared on the surface of the ink mark at 700 °C. It shows that more α -Fe₂O₃ was produced at this temperature, the width of the wear scar at 800 °C was narrowed and the surfaces also had a more obvious compaction layer and wear debris particles.

Raman spectroscopy was used to analyze the microstructure of material. Figure 13 and Table 1 show Raman spectra of the friction pair at 700 °C and 800 °C, respectively. All obvious peaks were listed. Raman spectra of the disc worn surface exhibited bands at 217 cm⁻¹, 281 cm⁻¹, 287 cm⁻¹, 397 cm⁻¹, 590 cm⁻¹, 644 cm⁻¹, 1304 cm⁻¹ and 1551 cm⁻¹ at 700 °C. Raman spectra of the ball worn surface exhibited bands at 219 cm⁻¹, 264 cm⁻¹, 319 cm⁻¹, 463 cm⁻¹, 642 cm⁻¹, 848 cm⁻¹, 1308 cm⁻¹ and 1555 cm⁻¹ at 700 °C. Raman spectra of the disc worn surface exhibited bands at 207 cm⁻¹, 225 cm⁻¹, 264 cm⁻¹, 291 cm⁻¹, 406 cm⁻¹, 613 cm⁻¹, 658 cm⁻¹, 1307 cm⁻¹ and 1554 cm⁻¹ at 800 °C. Raman spectra of the ball worn surface exhibited bands at 207 cm⁻¹, 264 cm⁻¹, 383 cm⁻¹, 574 cm⁻¹, 748 cm⁻¹, 852 cm⁻¹, 950 cm⁻¹, 1067 cm⁻¹, 1304 cm⁻¹, 1416 cm⁻¹, 1554 cm⁻¹ and 1764 cm⁻¹ at 800 °C.

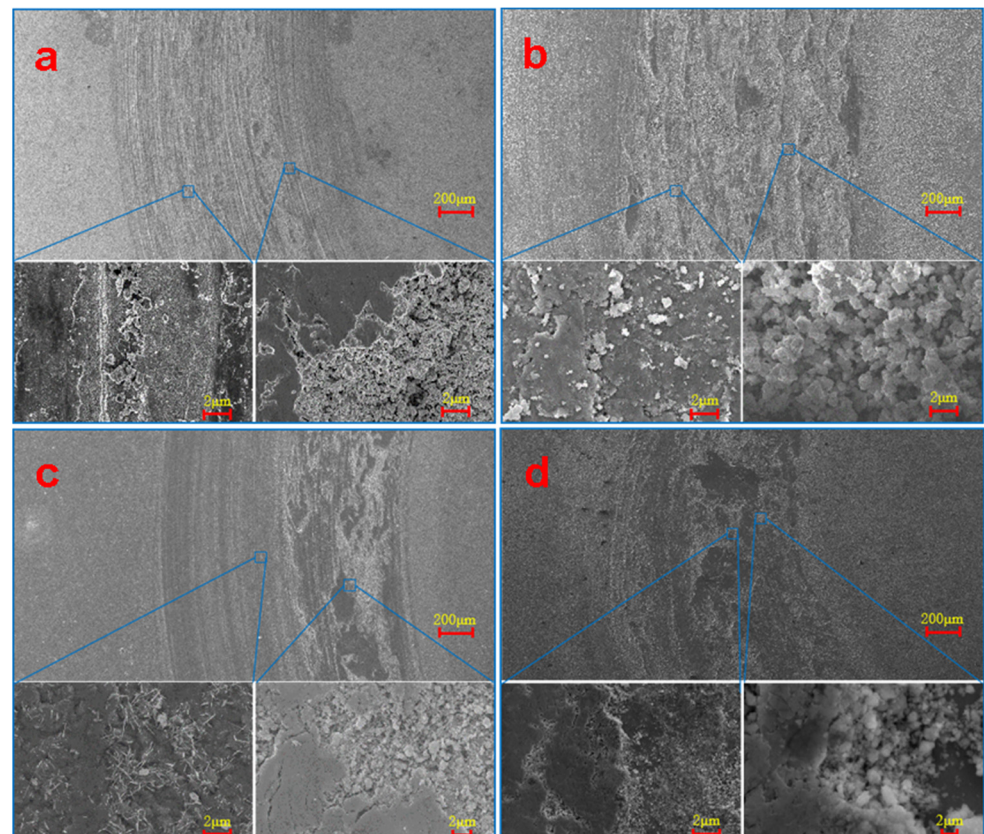


Figure 12. SEM images of the worn surface of BN coatings under different temperatures: (a) 500 °C, (b) 600 °C, (c) 700 °C and (d) 800 °C.

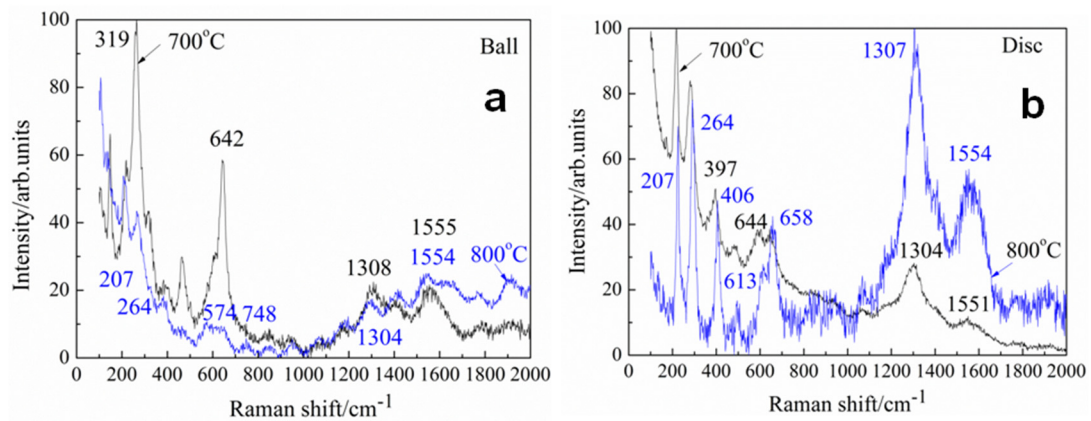


Figure 13. Raman spectra of the worn surface at 700 °C and 800 °C: (a) ball and (b) disc.

For the ball worn surface at 700 °C, the characteristic band was visible at position 642 cm^{-1} , which may be caused by TiO_2 [35]. The Raman spectra of 219 cm^{-1} and 319 cm^{-1} are characteristic of the hematite phase. The sharp and strong intensity band at 463 cm^{-1} indicates the metal oxygen (Fe-O) vibrations in hematite. Seen from the Raman spectra, $\alpha\text{-Fe}_2\text{O}_3$ exhibited 848 cm^{-1} [36]. The band at 1308 cm^{-1} may be assigned to $\gamma\text{-FeOOH}$ [37]. For the disc worn surface at 700 °C, TiO_2 was also characterized by bands at 397 and 644 cm^{-1} . The band at 1304 cm^{-1} is assigned to second harmonic vibrations of $\alpha\text{-Fe}_2\text{O}_3$. The hematite bands were clearly visible at 281 and 287 cm^{-1} derived from symmetric Fe-O bending mode. All these Raman peaks are attributed to the modes arising due to the presence of $\alpha\text{-Fe}_2\text{O}_3$.

Table 1. Raman spectra of friction pair at 700 °C and 800 °C.

FrictionPair Temperature (°C)	Ball		Disc	
	700 °C	800 °C	700 °C	800 °C
Wave shift (cm ⁻¹)		207	217	207
				225
		264	264	281
		319	383	287
		463	574	397
		642	748	590
		848	852	644
			950	
			1067	
		1308	1304	1304
			1416	
		1555	1554	1551
			1764	

For the worn surface at 800 °C, we assign the peaks at 207 and 264 cm⁻¹ to the Fe-O mode. For the disc worn surface at 800 °C, the peak at 658 cm⁻¹ is characteristic of Fe₃O₄. It can be clearly seen that the peaks appearing at 225, 291, 406 and 613 cm⁻¹ correspond to the characteristic peaks of α-Fe₂O₃. The wave number was measured at 1307 cm⁻¹, which represents the metal-oxygen stretching vibrations (Fe-O) and can be assigned to a cubic-phase of α-Fe₂O₃. For the ball worn surface at 800 °C, the 383 cm⁻¹ and 1304 cm⁻¹ bands are possibly assignable to α-Fe₂O₃, in agreement with the results of XRD. The peak at 1304 cm⁻¹ may be characteristic of γ-FeOOH, indicating that some of Fe₃O₄ are transformed into γ-FeOOH due to tribochemical reactions. The peak at 1554 cm⁻¹ is characteristic of γ-Fe₂O₃ [38]. This material is generated by the thermal dehydration of γ-FeOOH. The γ-Fe₂O₃ is partially transformed into α-Fe₂O₃, which is the most stable form of iron oxide. The transformation from γ-Fe₂O₃ to α-Fe₂O₃ occurred usually at 800 °C. Therefore, this phase transformation during the friction process could be due to an instantaneous high temperature. The Fe-N-O bending vibrations are located at 574 cm⁻¹ [39]. Other bands at 748 cm⁻¹ and 852 cm⁻¹ represent the Raman spectra of the iron complex. The peak at 1067 cm⁻¹ corresponds to Ti-O stretching modes. The band occurs a peak of 950 cm⁻¹, which is also the main band of iron titanium oxides [40]. In fact, when Ti-O bonds are present, they are the most prominent features at 1416 cm⁻¹.

There was α-Fe₂O₃ on the disc and ball worn surface at 700 °C and 800 °C, which is in agreement with XRD measurements. The γ-Fe₂O₃ peak was also detected from the disc worn surface at 800 °C. There was α-Fe₂O₃ and TiO₂ on the disc worn surface, and γ-FeOOH, α-Fe₂O₃ and TiO₂ on the ball worn surface at 700 °C. There was α-Fe₂O₃, Fe₃O₄ and γ-Fe₂O₃ on the disc worn surface, and α-Fe₂O₃, γ-FeOOH, γ-Fe₂O₃, Fe-N-O and TiO₂ on the ball worn surface at 800 °C. Therefore, it is considered that tribooxidation was the main reason leading to antifriction behavior of h-BN coatings.

The h-BN coatings were prepared on the steel substrate to improve high temperature tribological properties of steel. The h-BN coatings were partially worn out during sliding, or there were some cracks due to the thermal expansion between h-BN coatings and substrate under high temperature. The steel substrate was oxidized to iron oxides such as magnetite (Fe₃O₄), hematite (α-Fe₂O₃) and magnetic maghemite (γ-Fe₂O₃) according to thermodynamic calculation, as shown in Table 2. Fe₃O₄ was not stable in the ambient atmosphere, and further oxidized to α-Fe₂O₃ and γ-Fe₂O₃ at high temperature. According to XRD and Raman measurements, there was h-BN and α-Fe₂O₃ on the worn surface and Fe-N-O species were also observed. It is inferred that the composite of Fe₂O₃/h-BN is formed during sliding although there is also few B₂O₃. This composite is helpful to improve the high temperature antifriction behavior even high temperature superlubricity of the friction pair. Moreover, γ-Fe₂O₃ crystalline has FCC crystal microstructure and 12 kinds of slip plane, which leads to the good antifriction behaviors comparing with α-Fe₂O₃, which

is beneficial to achieve superlubricity at 800 °C. However, as shown in Figures 8 and 9, the wear debris were accumulated on the wear scar of disc and these wear debris were partially transferred to the worn surface of the ball, which may result in the fluctuation of CoF.

Table 2. The Gibbs free energy of the friction pair ($\Delta_r G_m^\theta$).

Reaction	500 °C	600 °C	700 °C	800 °C
$3\text{Fe} + 2\text{O}_2 = \text{Fe}_3\text{O}_4$	−857.39	−827.29	−797.67	−767.94
$4\text{Fe} + 3\text{O}_2 = 2\text{Fe}_2\text{O}_3$	−615.91	−590.77	−565.94	−541.16
$2\text{Fe} + \text{O}_2 = 2\text{FeO}$	−427.55	−414.64	−401.68	−388.52
$6\text{FeO} + \text{O}_2 = 2\text{Fe}_3\text{O}_4$	−432.13	−410.65	−390.31	−370.32
$4\text{Fe}_3\text{O}_4 + \text{O}_2 = 6\text{Fe}_2\text{O}_3$	−265.91	−235.47	−204.99	−175.23
$2\text{BN} + 3\text{H}_2\text{O} = \text{B}_2\text{O}_3 + 2\text{NH}_3$	−123.82	−130.50	−134.90	−137.25
$\text{B}_2\text{O}_3 + 3\text{H}_2\text{O} = 2\text{H}_3\text{BO}_3$	−2.67	7.27	18.62	31.23

High temperature friction results prove that h-BN is very suitable to be served as high temperature solid lubricant. The h-BN coatings show excellent high temperature tribological properties due to the intrinsic interlayer slipping reducing the sliding resistance. The superb chemical inertness and high temperature resistance of h-BN can be applied in many harsh conditions [41]. The h-BN has its distinctive advantages at 500 °C and above. The friction mechanism of h-BN coatings is attributed to the lamellar structures of h-BN at relatively low temperature. The lamellar structures have strong covalent bonds in the plane and weak van der Waals forces between the planes. During sliding, h-BN coatings were partially worn out and the steel substrate was unavoidably oxidized by oxygen in ambient environment at high temperature. There was $\alpha\text{-Fe}_2\text{O}_3$ on the worn surface of disc and ball according to XRD and Raman measurements. The $\alpha\text{-Fe}_2\text{O}_3$ were transferred and adhered to form a dense lubrication layer on the worn surface on ball, as shown in Figure 9, which makes low CoF of the friction system. Therefore, it is considered that the tribooxidation was the main reason leading to low CoF of the friction system [42–45]. Oxygen atoms tended to be embedded in B and N vacancies and reacted with B atoms to form B_2O_3 at high temperature. B_2O_3 was detected in the wear scar of disc at the temperatures of 500 °C, 700 °C and 800 °C. It is well known that h-BN can be functionalized with iron oxide [46]. At high temperature, there is much more friction heating, which improves the surface activity of h-BN. Therefore, the composite of $\alpha\text{-Fe}_2\text{O}_3$ and BN was generated in situ during sliding as h-BN is functionalized with $\alpha\text{-Fe}_2\text{O}_3$. The XRD measurement of the disc worn surface shows the characterization peaks of h-BN and $\alpha\text{-Fe}_2\text{O}_3$, which signifies $\alpha\text{-Fe}_2\text{O}_3$ was successfully prepared on the surface of h-BN. The h-BN is expected to be used as a supporter of $\alpha\text{-Fe}_2\text{O}_3$. The $\alpha\text{-Fe}_2\text{O}_3/\text{h-BN}$ composite achieves an excellent high temperature antifriction performance. Therefore, this composite combines the advantageous mechanical properties of $\alpha\text{-Fe}_2\text{O}_3$ and h-BN, forming the synergistic effect in improving high temperature tribological performances of h-BN coatings. The results verify that the hybrid materials exhibit the superior tribological performance than h-BN and $\alpha\text{-Fe}_2\text{O}_3$ alone.

At 500 °C, friction occurred between h-BN coatings and ZrO_2 at the initial stage. The initial CoF is high, about 0.39, because the friction occurred between h-BN and ZrO_2 ceramics. There may be a mismatch in thermal expansion and stress behavior of h-BN coatings and steel; therefore, the cracks were formed and oxygen was penetrated into coatings at high temperature. The oxides were generated on the disc due to high friction heating and oxides were partially transferred to the worn surface of ball. The steel substrate was oxidized to iron oxide, such as Fe_3O_4 , since the Gibbs free energy of the chemistry reaction of Fe_3O_4 is low at initial stage. However, Fe_3O_4 is easily oxidized into Fe_2O_3 in open air. The contact friction pair was iron oxide on ZrO_2 ball and the composite of $\alpha\text{-Fe}_2\text{O}_3/\text{h-BN}$; therefore, CoF decreased, although CoF fluctuated slightly and was relatively stable due to the good sliding between planes of h-BN with the increase in the sliding time. At the final stage, h-BN was oxidized to B_2O_3 according to XRD measurement under high friction heating and high environment temperature. The contact friction pair became $\alpha\text{-Fe}_2\text{O}_3$ on

ZrO₂ ball and the composite of α -Fe₂O₃/h-BN and B₂O₃; therefore, CoF decreased further to the minimum value around 1800s and increased slowly again along the sliding time. At 600 °C, there was Fe₃O₄ and α -Fe₂O₃ on the steel because the steel was sufficiently oxidized at higher temperature. The friction occurred between ZrO₂ on ball and mostly iron oxides with h-BN on steel at the initial stage, which causes a high initial CoF of 0.48 compared with that at 500 °C. It is interesting that there is more wear debris and the transferred films on ball at 600 °C. The transferred films are probably α -Fe₂O₃ [3] and covered evenly all the worn surfaces of ball, as shown in Figure 9b. CoF decreased to a low value with the adding of α -Fe₂O₃ on ball. The contact friction pair became α -Fe₂O₃ and ZrO₂ on ball and the composite of Fe₃O₄, α -Fe₂O₃ and h-BN, which is probably wrapped in iron oxides and as hardening phase due to high hardness, as shown in Figure 3. CoF increased slowly and fluctuated to a high value around 600 s with the full coverage of α -Fe₂O₃ on ball. At this point, the temperature at the friction interface was higher than 600 °C because there was high friction heating and the environmental temperature was 600 °C. It is well known that Fe₃O₄ is stable at high temperature and the transition from Fe₃O₄ to γ -Fe₂O₃ was performed at 650 °C [46]. The contact friction pair was α -Fe₂O₃ on ball and the composite of Fe₃O₄, γ -Fe₂O₃, α -Fe₂O₃ and h-BN on steel, which resulted in high CoF at this point. The γ -Fe₂O₃ acts as a soft solid lubricant between the contact surfaces at high temperature [47]. CoF decreased with increase in the transition from Fe₃O₄ to γ -Fe₂O₃ until all Fe₃O₄ was worn out. CoF decreased to the minimum value around 0.03 due to the phase transformation of iron oxides and increased slowly because the soft γ -Fe₂O₃ was possibly worn out and there was no more transition from Fe₃O₄ to γ -Fe₂O₃. It is surprising that there is no boron oxide according to XRD measurement, because h-BN was probably wrapped in iron oxides and the steel was much easily oxidized than h-BN according to Table 2. At the final stage, CoF was low because the contact pair was α -Fe₂O₃ on the ball and the composite of α -Fe₂O₃/h-BN according to XRD. With temperature reaching 700 °C, Ti was oxidized to TiO₂ according to Raman spectra and XRD measurement. Fe₃O₄ was oxidized to α -Fe₂O₃ and friction occurred between ZrO₂ on ball and the mixtures of iron oxides, TiO₂ and h-BN on steel, which results in a low initial CoF of 0.31. There were few oxides on the worn surface of the ball, as shown in Figures 9 and 13, and then α -Fe₂O₃ reacted with ZrO₂ to form the composite of α -Fe₂O₃/ZrO₂ under the synergistic effect of high friction heating and high environment temperature [3], which results in low CoF. CoF fluctuated with the sliding time and was relatively stable according to tribochemistry reaction of Fe, Ti and h-BN under high friction heating and high environment temperature. The average CoF was about 0.07 at final and stable stage. The contact pair was α -Fe₂O₃, TiO₂ and γ -FeOOH on ball and the composite of α -Fe₂O₃/h-BN, B₂O₃ and TiO₂ according to XRD and Raman spectra. The phase transition from metastable γ -Fe₂O₃ to stable α -Fe₂O₃ with rhombohedral crystal structure was approved at 800 °C. At 800 °C, there was mostly α -Fe₂O₃ on the disc surface. The contact pair was ZrO₂ on ball and the mixtures of iron oxides, h-BN and TiO₂, which leads to high initial CoF of 0.73. The iron oxide was transferred to ball and there is the tribochemistry reaction of h-BN, the formation of Fe-N-O and the phase transformation of iron oxide due to high friction heating and high environment temperature. CoF fluctuated and decreased to the minima value of 0.02 although CoF increased slightly. The contact pair was α -Fe₂O₃, TiO₂, γ -FeOOH, γ -Fe₂O₃ and Fe-N-O species on the ball and the mixtures of α -Fe₂O₃/h-BN, γ -Fe₂O₃, B₂O₃ and Fe₃O₄ on steel according to XRD and Raman spectra. There was complex tribooxidation and the phase transformation during sliding, resulting in high temperature superlubricity at 800 °C.

According to the analysis, the possible high temperature superlubricity mechanisms can be concluded as shown in Figure 14. Firstly, h-BN exhibits excellent antifriction behaviors inherently due to its unique lamellar structure. Secondly, Fe₂O₃, especially in γ -Fe₂O₃, has good high temperature plasticity and lubricity. Thirdly, α -Fe₂O₃ supported by h-BN plays an important synergistic effect in enhancing high temperature antifriction behavior. Finally, the friction occurred between the composite of α -Fe₂O₃/ZrO₂ on ball and the

composite of $\gamma\text{-Fe}_2\text{O}_3/\text{h-BN}$ on the disc, which results in high temperature superlubricity at $800\text{ }^\circ\text{C}$, although there maybe h-BN, oxides of Fe and Ti and boron oxide. Actually, these oxides of Fe and Ti, boron oxide and BN are beneficial to improve the high temperature tribological properties of steel, or not superlubricity in the friction system. Therefore, the composite of $\alpha\text{-Fe}_2\text{O}_3/\text{h-BN}$ against the composite of $\alpha\text{-Fe}_2\text{O}_3/\text{ZrO}_2$ can significantly improve high temperature antifriction behaviors of steel.

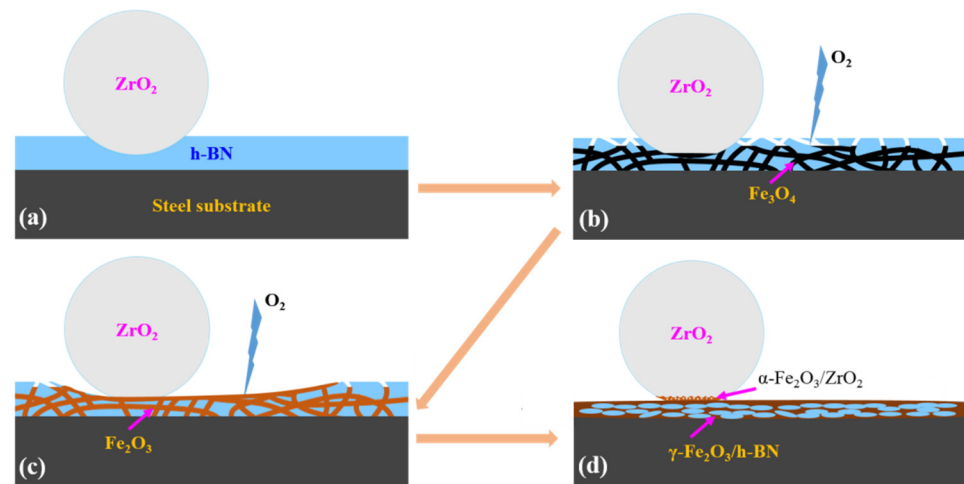


Figure 14. Schematic diagram of the friction process at $800\text{ }^\circ\text{C}$: (a) at initial stage, (b) the oxidation stage, (c) the phase change stage and (d) superlubricity stage.

4. Conclusions

The hexagonal boron nitride coatings were prepared on the steel substrate by using radio frequency magnetron sputtering technology. The tribological properties of hexagonal boron nitride coatings and the influence mechanism of temperature on the tribological properties were investigated. Microstructure, morphology, mechanics and high temperature low friction mechanism of h-BN coatings on steel were discussed in depth. These results provide significant theoretical and practical implications of h-BN coatings on steel and of great practical value in industries help to understand the tribological properties. The main findings in this work are summarized as follows:

- (1) The h-BN coatings are beneficial to improve the high temperature tribological properties of steel. CoFs of h-BN coatings are much lower than those of the uncoated steel at the same temperature;
- (2) The wear mechanism of h-BN coatings is tribooxidation, resulting in super low friction of the friction pair at high temperature. There are $\alpha\text{-Fe}_2\text{O}_3$, Fe_3O_4 and $\gamma\text{-Fe}_2\text{O}_3$ on the disc worn surface, and $\alpha\text{-Fe}_2\text{O}_3$, $\gamma\text{-FeOOH}$, $\gamma\text{-Fe}_2\text{O}_3$ and TiO_2 on the ball worn surface at $800\text{ }^\circ\text{C}$. The oxidation is the main factor for the antifriction and anti wear behavior of the friction pair at high temperature;
- (3) The h-BN coatings on steel exhibit high temperature superlubricity at $800\text{ }^\circ\text{C}$. CoFs of the friction pair are as super low as about 0.02 at $800\text{ }^\circ\text{C}$ at the stable stage. The superlubricity mechanism is attributed to the formation of the composite of $\gamma\text{-Fe}_2\text{O}_3/\text{h-BN}$ due to tribochemistry.

Funding: This research was funded by National Natural Science Foundation of China (51675409 and 51805409), National Science and Technology Major Project (j2019-IV-0004-0071) and the Natural Science Foundation of Chongqing, China (cstc2019jcyj-msxmX0577) and Natural Science Basic Research Plan in Shaanxi Province of China (2022JM-251).

Institutional Review Board Statement: Not applicable.

Informed Consent Statement: Not applicable.

Data Availability Statement: Not applicable.

Acknowledgments: Not applicable.

Conflicts of Interest: The authors declare no conflict of interest.

References

1. Trzepieciniski, T.; Lemu, H. Recent developments and trends in the friction testing for conventional sheet metal forming and incremental sheet forming. *Metals* **2019**, *10*, 47. [\[CrossRef\]](#)
2. Voevodin, A.; Zabinski, J. Nanocomposite and nanostructured tribological materials for space applications. *Compos. Sci. Technol.* **2005**, *65*, 741–748. [\[CrossRef\]](#)
3. Zeng, Q.; Zhu, J.; Long, Y.; Bouchet, M.I.d.; Martin, J.M. Transformation-induced high temperature low friction behaviors of ZrO₂-steel system at temperatures up to 900 °C. *Mater. Res. Express* **2019**, *6*, 0865f5. [\[CrossRef\]](#)
4. DellaCorte, C. The effect of counterface on the tribological performance of a high temperature solid lubricant composite from 25 to 650 °C. *Surf. Coat. Technol.* **1996**, *86*, 486–492. [\[CrossRef\]](#)
5. Zeng, Q. High-temperature superlubricity behaviors of γ -Fe₂O₃@SiO₂ nanocomposite coatings. In *Composite Materials*; Elsevier: Amsterdam, The Netherlands, 2021; pp. 489–501.
6. Nowak, P.; Kucharska, K.; Kamiński, M. Ecological and health effects of lubricant oils emitted into the environment. *Int. J. Environ. Res. Public Health* **2019**, *16*, 3002. [\[CrossRef\]](#)
7. Wu, Y.Y.; Tsui, W.C.; Liu, T.C. Experimental analysis of tribological properties of lubricating oils with nanoparticle additives. *Wear* **2007**, *262*, 819–825. [\[CrossRef\]](#)
8. Fontaine, J. Towards the use of diamond-like carbon solid lubricant coatings in vacuum and space environments. *Proc. Inst. Mech. Eng. Part J J. Eng. Tribol.* **2008**, *222*, 1015–1029. [\[CrossRef\]](#)
9. Zeng, Q.; Erdemir, A.; Eryilmaz, O. Ultralow friction of ZrO₂ ball sliding against DLC films under various environments. *Appl. Sci.* **2017**, *7*, 938. [\[CrossRef\]](#)
10. Liu, Y.; Yu, B.; Cao, Z.; Shi, P.; Zhou, N.; Zhang, B.; Zhang, J.; Qian, L. Probing superlubricity stability of hydrogenated diamond-like carbon film by varying sliding velocity. *Appl. Surf. Sci.* **2018**, *439*, 976–982. [\[CrossRef\]](#)
11. Vazirisereshk, M.; Martini, A.; Strubbe, D.; Baykara, M.Z. Solid lubrication with MoS₂: A review. *Lubricants* **2019**, *7*, 57. [\[CrossRef\]](#)
12. Manu, B.; Gupta, A.; Jayatissa, A. Tribological properties of 2D materials and composites—A review of recent advances. *Materials* **2021**, *14*, 1630. [\[CrossRef\]](#)
13. Zhu, L.; Wang, C.; Wang, H.; Xu, B.; Zhuang, D.; Liu, J.; Li, G. Microstructure and tribological properties of WS₂/MoS₂ multilayer films. *Appl. Surf. Sci.* **2012**, *258*, 1944–1948.
14. Uzoma, P.C.; Hu, H.; Khadem, M.; Penkov, O.V. Tribology of 2D nanomaterials: A review. *Coatings* **2020**, *10*, 897. [\[CrossRef\]](#)
15. Zhu, J.; Zeng, Q.; He, W.; Zhang, B.; Yan, C. Elevated-temperature super-lubrication performance analysis of dispersion-strengthened WSN coatings: Experimental research and first-principles calculation. *Surf. Coat. Technol.* **2021**, *406*, 126651. [\[CrossRef\]](#)
16. Zeng, Q.; Yu, F.; Dong, G. Superlubricity behaviors of Si₃N₄/DLC Films under PAO oil with nano boron nitride additive lubrication. *Surf. Interface Anal.* **2013**, *45*, 1283–1290. [\[CrossRef\]](#)
17. Podgornik, B.; Kosec, T.; Kocijan, A.; Donik, C. Tribological behaviour and lubrication performance of hexagonal boron nitride (h-BN) as a replacement for graphite in aluminium forming. *Tribol. Int.* **2015**, *81*, 267–275. [\[CrossRef\]](#)
18. Podgornik, B.; Kafexhiu, F.; Kosec, T.; Jerina, J.; Kalin, M. Friction and anti-galling properties of hexagonal boron nitride (h-BN) in aluminium forming. *Wear* **2017**, *388*, 2–8. [\[CrossRef\]](#)
19. Yuan, S.; Toury, B.; Benayoun, S. Novel chemical process for preparing h-BN solid lubricant coatings on titanium-based substrates for high temperature tribological applications. *Surf. Coat. Technol.* **2015**, *272*, 366–372. [\[CrossRef\]](#)
20. Li, J.; Luo, J. Advancements in superlubricity. *Sci. China Technol. Sci.* **2013**, *56*, 2877–2887. [\[CrossRef\]](#)
21. Niu, Z.; Chen, F.; Xiao, P.; Zhuan, L.; Lang, P.; Yang, L. Effect of h-BN addition on friction and wear properties of C/C-SiC composites fabricated by LSI. *Int. J. Appl. Ceram. Technol.* **2022**, *19*, 108–118. [\[CrossRef\]](#)
22. Chen, J.; Chen, J.; Wang, S.; Sun, Q.; Cheng, J.; Yu, Y.; Yang, J. Tribological properties of h-BN matrix solid-lubricating composites under elevated temperatures. *Tribol. Int.* **2020**, *148*, 106333. [\[CrossRef\]](#)
23. Chen, J.; Sun, Q.; Chen, W.; Zhu, S.; Li, W.; Cheng, J.; Yang, J. High-temperature tribological behaviors of ZrO₂/h-BN/SiC composite under air and vacuum environments. *Tribol. Int.* **2021**, *154*, 106748. [\[CrossRef\]](#)
24. Tyagi, R.; Xiong, D.; Li, J.; Dai, J. High-temperature friction and wear of Ag/h-BN-containing Ni-based composites against steel. *Tribol. Lett.* **2010**, *40*, 181–186. [\[CrossRef\]](#)
25. Zhang, D.; Cui, X.; Jin, G.; Song, Q.; Yuan, C.; Fang, Y. Microstructure and tribological performance of laser-cladded Ni60/h-BN coatings on Ti-6Al-4V alloy at high temperature. *Tribol. Trans.* **2019**, *62*, 779–788. [\[CrossRef\]](#)
26. Zhang, Y.; Wang, W.; Hu, Z.; Liu, K.; Chang, J. Investigation of hBN powder lubricating characteristics of die steel H13-ceramic Si₃N₄tribopairat 800 °C. *Proc. Inst. Mech. Eng. Part J J. Eng. Tribol.* **2020**, *234*, 622–631. [\[CrossRef\]](#)
27. Torres, H.; Podgornik, B.; Jovičević-Klug, M.; Ripoll, M.R. Compatibility of graphite, hBN and graphene with self-lubricating coatings and tool steel for high temperature aluminium forming. *Wear* **2022**, *490*, 204187. [\[CrossRef\]](#)

28. Wang, Y.; He, W.; Zeng, Q.; Zhu, J. Effects of multiple post weld heat treatments on microstructure and precipitate of fine grained heat affected zone of P91 weld. *Steel Res. Int.* **2019**, *90*, 1800607. [[CrossRef](#)]
29. Mukhtiar, S.; Hitesh, V.; Ravinder, K. Micro structural characterization of BN thin films using RF magnetron sputtering method. *Mater. Today Proc.* **2020**, *26*, 2277–2282.
30. Tran, T.; Chung, K. Tribological characteristics of single-layer h-BN measured by colloidal probe atomic force microscopy. *Coatings* **2020**, *10*, 530. [[CrossRef](#)]
31. Yang, Y.; Chen, J.; Guo, L.; Tan, D.; Zeng, Q.; Liu, Q.; Liu, K.; Chen, Z.; Zou, J.; Lu, D. Effects of initial texture on rolling texture and property of electrodeposited nickel plate. *J. Comput. Theor. Nanosci.* **2015**, *12*, 2643–2647. [[CrossRef](#)]
32. Zhao, Y.; Zhang, G.; Liang, M.; Zeng, Q. Study on the friction and wear performance of lightly loaded reciprocating carbon/aramid-based composites. *Adv. Mater. Sci. Eng.* **2021**, *2021*, 9924690. [[CrossRef](#)]
33. Nasr, M.; Soussan, L.; Viter, R.; Eid, C.; Habchi, R.; Miele, P.; Bechelany, M. High photo degradation and antibacterial activity of BN-Ag/TiO₂ composite nanofibers under visible light. *New J. Chem.* **2018**, *42*, 1250–1259. [[CrossRef](#)]
34. Yang, X.; Xu, L.; Choon, N.; Chen, S. Magnetic and electrical properties of poly pyrrole-coated γ -Fe₂O₃ nanocomposite particles. *Nanotechnology* **2003**, *14*, 624.
35. Khaldi, O.; Majouri, A.; Larbi, T. Theoretical and experimental investigation of the electronic, optical, electric, and elastic properties of Zn-doped anatase TiO₂ for photocatalytic applications. *Appl. Phys. A* **2021**, *127*, 1–8. [[CrossRef](#)]
36. Harraz, F.; Faisal, M.; Jalalah, M.; Almadiy, A.A.; Sayari, S.A. Conducting polythiophene/ α -Fe₂O₃ nanocomposite for efficient methanol electrochemical sensor. *Appl. Surf. Sci.* **2020**, *508*, 145226. [[CrossRef](#)]
37. Dong, H.; Zhao, F.; Zeng, G.; Tang, L.; Fan, C.; Zhang, L.; Zeng, Y.; He, Q.; Xie, Y.; Wu, Y. Aging study on carboxymethyl cellulose-coated zero-valent iron nanoparticles in water: Chemical transformation and structural evolution. *J. Hazard. Mater.* **2016**, *312*, 234–242. [[CrossRef](#)]
38. Tokubuchi, T.; Arbi, R.; Zhenhua, P.; Katayama, K.; Turak, A.; Sohn, W.Y. Enhanced photoelectrochemical water splitting efficiency of hematite (α -Fe₂O₃)-Based photoelectrode by the introduction of maghemite (γ -Fe₂O₃) nanoparticles. *J. Photochem. Photobiol. A Chem.* **2021**, *410*, 113179. [[CrossRef](#)]
39. Benko, B.; Yu, N. Resonance Raman studies of nitric oxide binding to ferric and ferrous hemoproteins: Detection of Fe (III)-NO stretching, Fe (III)-N-O bending, and Fe (II)-N-O bending vibrations. *Proc. Natl. Acad. Sci. USA* **1983**, *80*, 7042–7046. [[CrossRef](#)]
40. Leon, Y.; Lofrumento, C.; Zoppi, A.; Carles, R.; Castellucci, E.M.; Sciau, P. Micro-Raman investigation of terra sigillata slips: A comparative study of central Italian and southern Gaul productions. *J. Raman Spectrosc.* **2010**, *41*, 1550–1555. [[CrossRef](#)]
41. Zhang, R.; Ding, Q.; Yang, L.; Zhang, S.; Niu, Q.; Ye, J. A novel sonogel based on h-BN nanosheets for the tribological application under extreme conditions. *Tribol. Int.* **2019**, *138*, 271–278. [[CrossRef](#)]
42. Lavrenko, V.; Alexeev, A. High-temperature oxidation of boron nitride. *Ceram. Int.* **1986**, *12*, 25–31. [[CrossRef](#)]
43. Zeng, Q.; Qin, L. High temperature anti-friction behaviors of a-Si: H films and counterface material selection. *Coatings* **2019**, *9*, 450–460. [[CrossRef](#)]
44. Zeng, Q.; Chen, T. Superlow friction and oxidation analysis of hydrogenated amorphous silicon films under high temperature. *J. Non-Cryst. Solids* **2018**, *493*, 73–81. [[CrossRef](#)]
45. Zeng, Q.; Erdemir, A.; Eryilmaz, O. Superlubricity of the DLC films-related friction system at elevated temperature. *RSC Adv.* **2015**, *5*, 93147–93154. [[CrossRef](#)]
46. Thangasamy, P.; Sathish, M. Dwindling the re-stacking by simultaneous exfoliation of boron nitride and decoration of α -Fe₂O₃ nanoparticles using a solvo thermal route. *New J. Chem.* **2018**, *42*, 5090–5095. [[CrossRef](#)]
47. Kazeminezhad, I.; Mosivand, S. Phase transition of electro oxidized Fe₃O₄ to γ and α -Fe₂O₃ nano particles using sintering treatment. *Acta Phys. Pol. A* **2014**, *125*, 1210–1214. [[CrossRef](#)]